# Experimental Evidence of Intrinsic Current Generation by Turbulence in Stationary Tokamak Plasmas

Erzhong Li,[1] X. L. Zou,[2] L. Q. Xu,[1,*] Y. Q. Chu,[1,3] X. Feng,[3] H. Lian,[4] H. Q. Liu,[1] A. D. Liu,[3] M. K. Han,[5] J. Q. Dong,[5] H. H. Wang,[1] J. W. Liu,[1,3] Q. Zang,[1] S. X. Wang,[1] T. F. Zhou,[1] Y. H. Huang,[6] L. Q. Hu,[1] C. Zhou,[3] H. X. Qu,[1,3] Y. Chen,[1,3] S. Y. Lin,[1] B. Zhang,[1] J. P. Qian,[1] J. S. Hu,[1] G. S. Xu,[1] J. L. Chen,[1] K. Lu,[1] F. K. Liu,[1] Y. T. Song,[1] J. G. Li,[1] and X. Z. Gong[1,†]

EAST Team

[1]*Institute of Plasma Physics, Chinese Academy of Sciences, Hefei 230031, People's Republic of China*
[2]*CEA, IRFM, F-13108 Saint-Paul-lez-Durance, France*
[3]*University of Science and Technology of China, Hefei 230022, People's Republic of China*
[4]*University of California Los Angeles, Los Angeles, California 90095, USA*
[5]*Southwestern Institute of Physics, P.O. Box 432, Chengdu 610041, People's Republic of China*
[6]*Advanced Energy Research Center, Shenzhen University, Shenzhen 518060, People's Republic of China*

(Received 28 January 2021; revised 16 September 2021; accepted 1 February 2022; published 25 February 2022)

High-$\beta_{\theta e}$ (a ratio of the electron thermal pressure to the poloidal magnetic pressure) steady-state long-pulse plasmas with steep central electron temperature gradient are achieved in the Experimental Advanced Superconducting Tokamak. An intrinsic current is observed to be modulated by turbulence driven by the electron temperature gradient. This turbulent current is generated in the countercurrent direction and can reach a maximum ratio of 25% of the bootstrap current. Gyrokinetic simulations and experimental observations indicate that the turbulence is the electron temperature gradient mode (ETG). The dominant mechanism for the turbulent current generation is due to the divergence of ETG-driven residual flux of current. Good agreement has been found between experiments and theory for the critical value of the electron temperature gradient triggering ETG and for the level of the turbulent current. The maximum values of turbulent current and electron temperature gradient lead to the destabilization of an $m/n = 1/1$ kink mode, which by counteraction reduces the turbulence level ($m$ and $n$ are the poloidal and toroidal mode number, respectively). These observations suggest that the self-regulation system including turbulence, turbulent current, and kink mode is a contributing mechanism for sustaining the steady-state long-pulse high-$\beta_{\theta e}$ regime.

DOI: 10.1103/PhysRevLett.128.085003

*Introduction.*—Turbulence and magnetohydrodynamic (MHD) modes are common phenomena in astrophysical and laboratorial magnetized plasmas [1–4]. Multiscale instabilities are particularly important and have been widely studied in tokamaks [5–12]. It is shown that the magnetic shear or the plasma current profile plays a vital role for the control of turbulence and MHD [13,14]. In particular, the plasma self-generated current, such as the pressure-gradient-driven bootstrap current, is essential for a fusion reactor [15]. Recently, theories and simulations have predicted the generation of intrinsic current by turbulence due to the symmetry breaking of the turbulence spectrum [16–18], including the ion temperature-gradient-driven mode [19], trapped electron mode (TEM) [20], and electron temperature-gradient-driven mode (ETG) [21]. This intrinsic current is not yet experimentally observed. In this Letter, for the first time, the turbulent current is evidenced in current density measurements from a polarimeter-interferometer diagnostic in high-$\beta_{\theta e}$ plasmas [$\beta_{\theta e0} = p_{e0}/(B_{\theta 0}^2/2\mu_0) \approx 3$]. It is found that a MHD mode is excited once the turbulent current reaches about 25% of the bootstrap current and this, in return, regulates the turbulence and the turbulent current.

*Observations.*—High-$\beta_{\theta e}$ plasmas with steep central electron temperature gradient have been achieved by electron cyclotron resonance heating (ECRH) and low hybrid current drive (LHCD) on the Experimental Advanced Superconducting Tokamak (a major radius $R_0 = 1.75$ m, a minor radius $a = 0.45$ m, and the toroidal magnetic field $B_0 = 2.6$ T). The central electron temperature is $T_{e0} \sim 9$ keV and the normalized electron temperature gradient ($R/L_{Te} = -(R/T_e)\nabla T_e$) is ~10, much higher than the general case ($R/L_{Te} \sim 3$). This is caused by the ECRH due to its highly localized power deposition ($\rho_{\mathrm{dep}} < 0.2$). The achievement of high-$\beta_{\theta e}$ plasmas generally depends on the turbulence level and the MHD

 

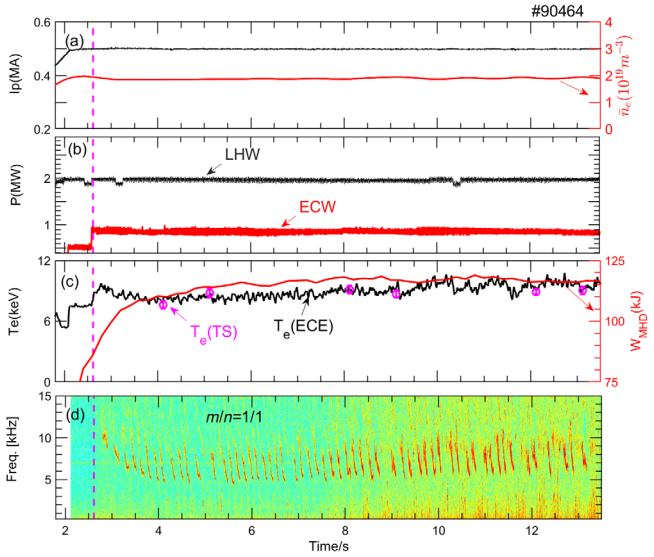


FIG. 1. Main plasma parameters in a typical shot No. 90464. (a) Plasma current and the line-averaged density, (b) low hybrid wave (LHW) and electron cyclotron wave (ECW) power, (c) central electron temperature measured by Electron Cyclotron Emission (ECE, solid line) and Thomson Scattering (TS, circle) and plasma stored energy ($W_{\mathrm{MHD}}$), and (d) time frequency spectrum of soft x-ray radiation across the core.

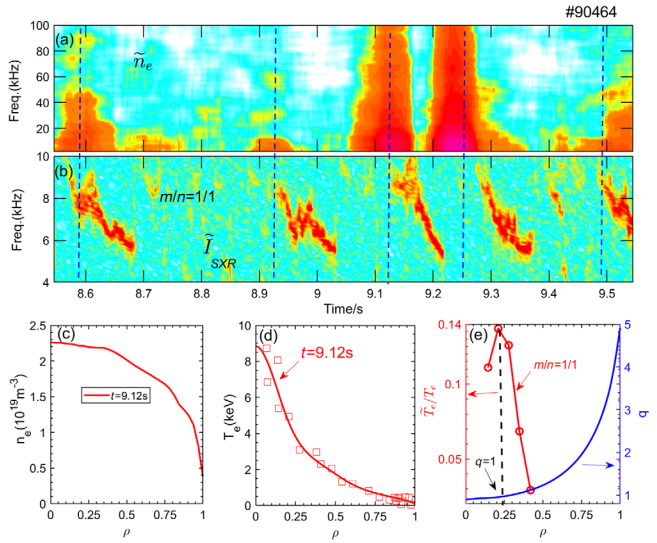


FIG. 2. Experimental observations. (a) The time frequency spectrum of electron density fluctuations. (b) Frequency spectrogram of soft x-ray perturbations. (c) Electron density profile. (d) Electron temperature profile. (e) $q$ profile and the $m/n = 1/1$ kink-mode-induced electron temperature perturbation.

activity. Figure 1 shows a typical long-duration discharge. The plasma current is $Ip = 0.5$ MA and the line-averaged electron density is $\bar{n}_e = 2 \times 10^{19}$ m$^{-3}$ [Fig. 1(a)]. The ECRH and LHCD powers are 0.9 and 2 MW, respectively [Fig. 1(b)]. The central electron temperature reaches $T_{e0} \sim 9$ keV ($\beta_{\theta e0} \approx 3$) and the plasma stored energy is about $W_{\mathrm{MHD}} \approx 115$ kJ in Fig. 1(c). The spectrum of the soft x-ray radiation (SXR) central chord signal shows an $m/n = 1/1$ mode (beginning time indicated by a vertical dash line) as seen in Fig. 1(d). The central ion temperature is nearly constant ($T_{i0} \sim 0.8$ keV). The small ratio of $T_{i0}/T_{e0}$ results from the very low level of energy exchange between electron and ion due to the low collisionality (low $n_e$, high $T_e$) in a purely electron heated plasma to obtain high LHCD current drive efficiency.

The electron temperature and the density profiles are measured by a Thomson scattering system and an interferometer system, respectively. The current profile can be obtained by a Faraday-effect polarimeter-interferometer system [22]. This system has 11 chords horizontally passing the vacuum vessel, which measures the electron density and the Faraday rotation angle, simultaneously. The vertical distance is 8.5 cm between two neighboring chords [23]. The density fluctuation or turbulence is measured by the Doppler backscattering system with $X$ mode polarization at the poloidal wave number $k_\theta \sim 6$ cm$^{-1}$ [24]. Figure 2(a) presents the frequency spectrogram of density fluctuations, showing turbulence bursts. Figure 2(b) shows the frequency spectrogram of the SXR signal, illustrating the $m/n = 1/1$ mode frequency chirping down from 8 to 6 kHz following each turbulence burst. The SXR perturbation comes from the $m/n = 1/1$ mode-induced $T_e$ and/or $n_e$ oscillation, while impurity contribution is negligible with well-coated plasma facing components. Figures 2(c) and 2(d) display the $T_e$ and $n_e$ profiles, respectively, showing that the central $T_e$ is steep and the $n_e$ is rather flat. The temperature perturbation ($\tilde{T}_e$) caused by the $m/n = 1/1$ mode is plotted in Fig. 2(e) where the safety factor ($q$) profile is also shown. The $m/n = 1/1$ resonant surface ($\rho_{1/1} \sim 0.25$) is clearly in the steep gradient region. The $\tilde{T}_e$ profile is of even symmetry around the $q = 1$, indicating a kink mode, and the spatial scale of this mode is $\delta\rho \sim 0.2$. The location of the turbulence measurement is close to $\rho_{1/1}$ and remains nearly constant because the density perturbation is very small and the density profile is almost unchanged. It should be emphasized that both turbulence and $m/n = 1/1$ kink mode are intermittent and that their amplitudes are modulated as indicated by the dash lines. These suggest that there exists a strong interaction between them and a correlation to the steep temperature gradient.

The periodic turbulence bursts and the $m/n = 1/1$ mode are further illustrated in Fig. 3. The turbulence is driven by $R/L_{Te}$, and its amplitude $A_{\mathrm{tur}}$ increases with $R/L_{Te}$ as shown in Figs. 3(a) and 3(b). $A_{\mathrm{tur}}$ is obtained from backscattering the amplitude signal by density fluctuations with frequency integral over 10–100 kHz. As $A_{\mathrm{tur}}$ reaches maximum, the $m/n = 1/1$ mode is destabilized which causes a decrease of both $R/L_{Te}$ and $A_{\mathrm{tur}}$. The mode frequency is far lower than the precession frequency

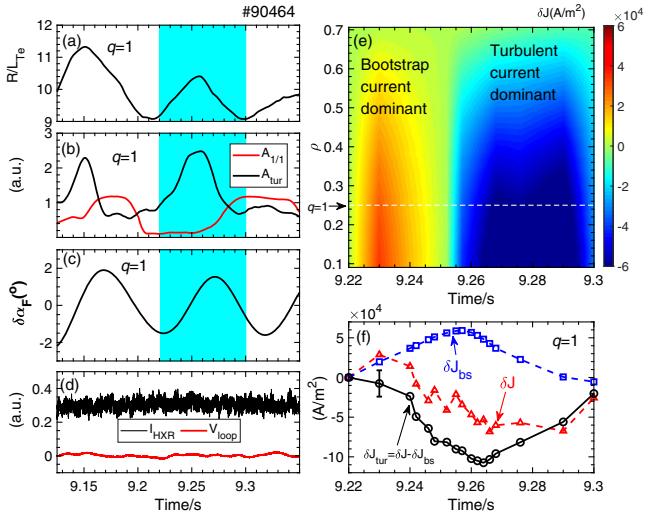


FIG. 3. Identification of turbulent current. (a) The normalized electron temperature gradient at $q = 1$. (b) The amplitudes of turbulence and $m/n = 1/1$ mode. (c) The measured perturbation of Faraday angle at $q = 1$. (d) The hard x-ray (HXR) signal and the loop voltage. (e) The time evolution of total current perturbation profile. (f) The total current perturbation at $q = 1$ (triangle symbol), the bootstrap current perturbation (square symbol), and the turbulent current (circle symbol) in a turbulence burst period.

($f_{D,EP} \approx 30$ kHz) of energetic electrons [25]. Thus, the mode destabilization is related to the plasma current or the pressure gradient.

The plasma current density ($J$) is composed of the Ohmic current ($J_{\mathrm{Oh}}$), the lower hybrid wave-driven current ($J_{\mathrm{LH}}$), and the gradient-driven bootstrap current ($J_{\mathrm{bs}}$), which are relevant to the loop voltage [26], fast electrons [27], and pressure gradient [28,29], respectively. It can be obtained from the polarimetry measured Faraday angle via $\alpha_F \sim \int n_e \vec{B}_\theta \cdot d\vec{l}$. $\vec{B}_\theta$ is the poloidal magnetic field along the sight chord, which is used in obtaining $J(t,\rho)$ by the Faraday rotation reconstruction algorithm with $129 \times 129$ spatial grids [30]. After the inversion, the spatial resolution is about ~0.6 cm. Figure 3(c) displays the time evolution of the Faraday angle perturbation. As the electron density remains nearly constant, the Faraday angle perturbation actually represents a modulation of plasma current. As shown in Fig. 3(d), no oscillation is observed on the hard x ray from fast electron bremsstrahlung. This implies that $J_{\mathrm{LH}}$ is unchanged. In addition, the loop voltage is zero, so that $J_{\mathrm{Oh}}$ can be neglected. Thus, the plasma current perturbation could be generated by the plasma itself.

Here, we define the current density profile at $t = 9.22$ s as the reference $J_0(\rho)$ when $R/L_{Te}$ is at the minimum (~9). As $R/L_{Te}$ increases above the minimum, the current density perturbation is calculated by $\delta J(t,\rho) = J(t,\rho) - J_0(\rho)$. The bootstrap current is obtained by the ONETWO code [31] with experimental profiles, and the ratio is $J_{\mathrm{bs}}/J_0|_{q=1} \approx 0.2$. Figure 3(e) shows $\delta J(t,\rho)$ during one period from $t = 9.22$ to 9.3 s, clearly indicating a positive current perturbation (cocurrent) preceding a negative current perturbation (countercurrent). Figure 3(f) shows that the bootstrap current perturbation is positive ($\delta J_{\mathrm{bs}} > 0$), while the measured $\delta J$ is mainly negative and almost in the opposite phase with $\delta J_{\mathrm{bs}}$. In the current timescale, the plasma self-inductance effect cannot change the positive bootstrap current perturbation into the countercurrent direction. These demonstrate that the experimentally observed negative current perturbation is not due to $\delta J_{\mathrm{bs}}$. The fact that the current perturbation is strongly correlated to the turbulence modulation suggests that the difference between $\delta J$ and $\delta J_{\mathrm{bs}}$ is caused by a turbulence-driven current.

The turbulence-driven current is defined as $\delta J_{\mathrm{tur}} = \delta J(t,\rho) - \delta J_{\mathrm{bs}}$. The time evolution of $\delta J_{\mathrm{tur}}$ at the $q = 1$ is presented in Fig. 3(f) (circle symbol) where $\delta J_{\mathrm{tur}}$ is negative, indicating the countercurrent direction. The maximum of $|\delta J_{\mathrm{tur}}|$ reaches ~100 kA/m$^2$, significantly surpassing $\delta J_{\mathrm{bs}} \sim 60$ kA/m$^2$. The positive current perturbation in Fig. 3(e) corresponds to the bootstrap current dominant phase, while the negative current perturbation corresponds to the turbulent current dominant phase.

Figure 4(a) represents the turbulence amplitude as a function of $R/L_{Te}$, basically showing a linear relationship. The turbulence could be the ETG [32] or the TEM [33]. The linear stability analysis is performed with an electromagnetic gyrokinetic code (HD7 [34]). The ion sound Larmor radius is $\rho_s = 0.54$ cm at $q = 1$ corresponding to $k_\theta \rho_s = 3.2$. Figures 4(b) and 4(d) show the growth rates of

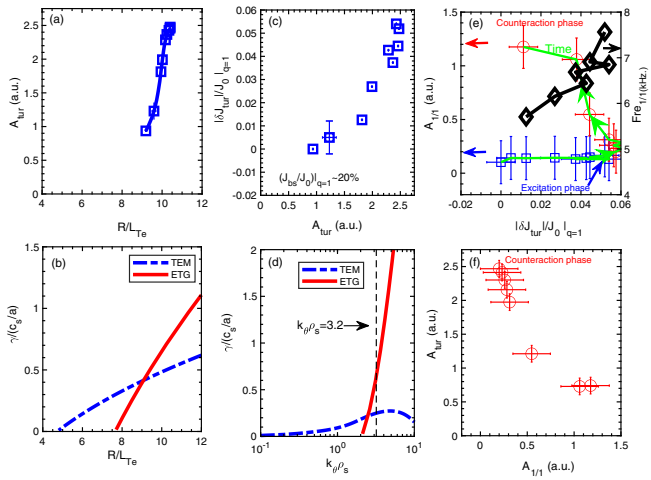


FIG. 4. Self-regulation system. (a) The measured turbulence amplitude plotted as a function of the normalized electron temperature gradient. (b) Growth rates of ETG and TEM at $k_\theta \rho_s = 3.2$ ($c_s$, the acoustic velocity). (c) The measured turbulent current dependency on the turbulence amplitude. (d) ETG and TEM $k_\theta$ spectra at $R/L_{Te} = 10$. (e) The $m/n = 1/1$ mode amplitude (left) and frequency (right) versus the turbulent current (green arrow indicates the time direction). (f) The turbulence amplitude with respect to the $m/n = 1/1$ mode amplitude.

turbulence as a function of $R/L_{Te}$ at $k_\theta\rho_s = 3.2$ and of $k_\theta\rho_s$ at $R/L_{Te} = 10$, respectively. The TEM $k_\theta$ spectrum covers a much larger area due to large $R/L_{Te}$. The ETG $k_\theta$ spectrum is at $k_\theta\rho_s > 2$ and dominant for $k_\theta\rho_s > 2.6$. At $k_\theta\rho_s = 3.2$, the ETG growth rate is much larger than that of TEM, indicating that the dominant turbulence is likely ETG. Furthermore, as shown in Fig. 4(b), the critical value of $R/L_{Te}$ for triggering ETG is about eight, which is very close to the experimental value shown in Fig. 4(a), while the critical value for triggering TEM is much lower. In contrast to TEM [35], the ETG has very little effect on the particle transport and electron density due to its small radial correlation length. These indicate that the observed turbulence bursts are most likely the ETG. As the $k_\theta$ spectrum does not change too much in the experimental range of $R/L_{Te} = 9 \sim 10$, the measurement at $k_\theta\rho_s \approx 3.2$ can be regarded as representative for the whole spectrum of turbulence.

In Fig. 4(c), the ratio of the turbulent current to the total current is plotted with respect to the turbulence amplitude. The maximum of $|\delta J_{\rm tur}|$ can reach about 5% of $J_0$ (25% of $J_{\rm bs}$). So far, several mechanisms are suggested, such as the trapped-passing electron boundary influenced by turbulence, the divergence of the residual turbulent flux ($\Gamma^{\rm res}$) and/or the turbulent forcing source ($S^{\rm res}$) [17–21]. The turbulence scattering of trapped into passing electrons would increase the cocurrent portion, in contrast to the current reduction with $R/L_{Te}$ increasing. Because the plasma loop voltage is zero, the pinch flux due to the parallel electric field may be negligible [36]. Thus, the observed turbulent current could be due to $\Gamma^{\rm res}$ and/or $S^{\rm res}$. For the ETG, their contributions are given by $\delta J_\Gamma = C_N J_{\rm bs}[\mp \Gamma^{\rm res}/(5\nu_{ei}\sqrt{\rho_e L_n})]\sqrt{a/R_0}$ and $\delta J_S = C_N J_{\rm bs}(S^{\rm res}/5\nu_{ei})\sqrt{a/R_0}$, respectively [21]. The sign $\mp$ corresponds to the positive or negative gradient of $\Gamma^{\rm res}$, and $C_N = L_p/eqn_e V_{\perp e}\rho_e$, where $V_{\perp e}$ is the electron thermal velocity, $\rho_e$ is the electron Larmor radius, and $\nu_{ei}$ is the electron-ion collision frequency. It should be noted that $\Gamma^{\rm res}$ and $S^{\rm res}$ require a finite parallel wave number (symmetry breaking), which is estimated as $\bar{k}_\parallel R = sk_\theta(w_k^2/L_I)$ ($w_k = 1/k_\theta$ is the mode width; $s$ is the magnetic shear). Experimental values at the $q = 1$ are $T_e \approx 4$ keV, $n_e \approx 2\times10^{19}$ m$^{-3}$, $V_{\perp e} = 2.7\times10^7$ m/s, $\rho_e = 8.9\times10^{-5}$ m, $\nu_{ei} = 4.3$ kHz, $\delta n_e/n_e \sim 0.8\%$, $R/L_{Te} \approx 10$, $s = 0.13$, $R/L_n \approx 0.3$, $L_I \approx L_p \approx L_{Te} \approx 0.2$ m, and $I_{\rm tur} \approx |\delta\hat{\phi}_k|^2 \approx (\delta n_e/n_e)^2 \sim 6.4\times10^{-5}$. $\delta n_e/n_e$ is deduced from the phase fluctuation measured by reflectometry [37]. In combination with simulations, one can obtain $\Gamma^{\rm res} \approx 1.38\times10^7$ A/ms and $S^{\rm res} \approx 2.14\times10^8$ A/m$^2$ s. The turbulent current due to $\Gamma^{\rm res}$ is $|\delta J_\Gamma/J_{\rm bs}|_{q=1} \sim 29.4\%$ and due to $S^{\rm res}$ is $|\delta J_S/J_{\rm bs}|_{q=1} \sim 10.8\%$. The measured value of $|\delta J_{\rm tur}/J_{\rm bs}|_{q=1} \sim 25\%$ is very close to the predicted value due to $\Gamma^{\rm res}$. In addition, the measured turbulent current is in the countercurrent (negative) direction. Thus, the observed turbulent current is mainly due to the ETG-driven residual turbulent flux. The rapid extension of the turbulent current with initial velocity $\bar{V}_r \sim 450$ m/s observed in Fig. 3(e) could be explained by the turbulence spreading. Indeed, $\bar{V}_r$ is quite close to the ballistic front velocity characterizing the turbulence spreading $V_f = \sqrt{\chi_e\gamma} \sim 548$ m/s [38], where we use the spectrum-averaged growth rate $\gamma \approx 3\times10^5$ s$^{-1}$ over $k_\theta\rho_s = 2$–3.2 shown in Fig. 4(d) and the electron heat diffusivity $\chi_e \approx \rho_e V_{\perp e}(\rho_e/L_{Te}) \approx 1.0$ m$^2$/s [39].

Figure 4(e) represents the dependency of $m/n = 1/1$ mode on the turbulent current, showing a critical value of the temperature gradient or the turbulent current for the mode excitation. The mode is destabilized due to the high-temperature gradient in a low magnetic shear regime, resulting from the turbulent countercurrent. The frequency chirping down is caused by the reduction of diamagnetic rotation due to the decrease of the temperature gradient. Figure 4(f) shows that the growing $m/n = 1/1$ mode decreases the level of turbulence and the electron temperature gradient by releasing free energy. This naturally reduces the turbulent current, showing a counteraction.

In conclusion, the turbulence-driven current has been experimentally observed, which is generated in the countercurrent direction and can reach 25% of the bootstrap current. This value is very close to that predicted by theory, showing that the dominant mechanism for turbulent current generation is due to the divergence of ETG-driven residual turbulent flux of current. The self-regulation system among the ETG turbulence, turbulent current, and $m/n = 1/1$ kink mode plays a contributing role for sustaining the stationary high-$\beta_{\theta e}$ long-pulse plasmas. This Letter has important implications for the multiscale interaction physics and the central current profile control in the future fusion reactor.

Professor W. X. Ding (USTC, China) is acknowledged for fruitful discussions. E. L. also wants to thank Dr. Max E. Austin (University of Texas at Austin), Professor Lu Wang (HUST, China), and Professor H. S. Cai (USTC, China) for helpful discussions. This work is supported by the Youth Innovation Promotion Association Chinese Academy of Sciences under Grant No. 2018483 and partly by the National Key R&D Program of China (Grant No. 2019YFE03010002).

*lqxu@ipp.ac.cn
†xz_gong@ipp.ac.cn

[1] B. Coppi, M. N. Rosenbluth, and R. Sagdeev, Phys. Fluids **10**, 582 (1967).
[2] A. L. Moser and P. M. Bellan, Nature (London) **482**, 379 (2012).
[3] N. Nishizuka and K. Shibata, Phys. Rev. Lett. **110**, 051101 (2013).
[4] J. W. Connor, J. B. Taylor, and H. R. Wilson, Phys. Rev. Lett. **70**, 1803 (1993).

[5] E. Mazzucato, Phys. Rev. Lett. **36**, 792 (1976).
[6] G. W. Hammett and F. W. Perkins, Phys. Rev. Lett. **64**, 3019 (1990).
[7] R. E. Waltz, J. C. DeBoo, and M. N. Rosenbluth, Phys. Rev. Lett. **65**, 2390 (1990).
[8] P. H. Diamond, V. B. Lebedev, D. E. Newman, B. A. Carreras, T. S. Hahm, W. M. Tang, G. Rewoldt, and K. Avinash, Phys. Rev. Lett. **78**, 1472 (1997).
[9] S.-I. Itoh, K. Itoh, and M. Yagi, Phys. Rev. Lett. **91**, 045003 (2003).
[10] K. W. Gentle, M. E. Austin, J. C. DeBoo, T. C. Luce, and C. C. Petty, Phys. Plasmas **13**, 012311 (2006).
[11] L. Bardoczi, T. L. Rhodes, T. A. Carter, A. B. Navarro, W. A. Peebles, F. Jenko, and G. McKee, Phys. Rev. Lett. **116**, 215001 (2016).
[12] P. H. Diamond, S.-I. Itoh, K. Itoh, and T. S. Hahm, Plasma Phys. Contr. Fusion **47**, R35 (2005).
[13] G. T. Hoang *et al.*, Nucl. Fusion **34**, 75 (1994).
[14] W. Horton, Rev. Mod. Phys. **71**, 735 (1999).
[15] M. Kikuchi and M. Azumi, Rev. Mod. Phys. **84**, 1807 (2012).
[16] F. L. Hinton, R. E. Waltz, and J. Candy, Phys. Plasmas **11**, 2433 (2004).
[17] C. J. McDevitt, X. Z. Tang, and Z. Guo, Phys. Rev. Lett. **111**, 205002 (2013).
[18] X. Garbet *et al.*, J. Phys. **561**, 012007 (2014).
[19] C. J. McDevitt, X. Z. Tang, and Z. H. Guo, Phys. Plasmas **24**, 082307 (2017).
[20] W. X. Wang, T. S. Hahm, E. A. Startsev, S. Ethier, J. Chen, M. G. Yoo, and C. H. Ma, Nucl. Fusion **59**, 084002 (2019).
[21] W. He, L. Wang, S. Peng, W. Guo, and G. Zhuang, Nucl. Fusion **58**, 106004 (2018).
[22] H. Q. Liu *et al.*, Rev. Sci. Instrum. **85**, 11D405 (2014).
[23] H. Q. Liu *et al.*, Rev. Sci. Instrum. **87**, 11D903 (2016).
[24] X. Feng *et al.*, Rev. Sci. Instrum. **90**, 024704 (2019).
[25] R. B. White, L. Chen, F. Romanelli, and R. Hay, Phys. Fluids **28**, 278 (1985).
[26] L. Spitzer, *Physics of Fully Ionized Gases* (Interscience, New York, 1962).
[27] N. J. Fisch, Rev. Mod. Phys. **59**, 175 (1987).
[28] M. N. Rosenbluth, R. D. Hazeltine, and F. L. Hinton, Phys. Fluids **15**, 116 (1972).
[29] H. R. Wilson, Nucl. Fusion **32**, 257 (1992).
[30] J. Qian *et al.*, Nucl. Fusion **57**, 036008 (2017).
[31] W. Pfeiffer, W. Davidson, R. Miller, and R. Waltz, ONETWO: A computer code for modeling plasma transport in tokamaks, Technical Report No. GAA-16178, General Atomics, San Diego, 1980.
[32] Y. C. Lee, J. Q. Dong, P. N. Guzdar, and C. S. Liu, Phys. Fluids **30**, 1331 (1987).
[33] H. Nordman, J. Weiland, and A. Jarmén, Nucl. Fusion **30**, 983 (1990).
[34] J. Q. Dong, H. Sanuki, K. Itoh, and L. Chen, Phys. Plasmas **9**, 4699 (2002).
[35] W. L. Zhong, X. L. Zou, C. Bourdelle, S. D. Song, J. F. Artaud, T. Aniel, and X. R. Duan, Phys. Rev. Lett. **111**, 265001 (2013).
[36] W. X. Ding, L. Lin, D. L. Brower, A. F. Almagri, B. E. Chapman, G. Fiksel, D. J. DenHartog, and J. S. Sarff, Phys. Rev. Lett. **110**, 065008 (2013).
[37] C. Fanack, I. Boucher, F. Clairet, S. Heuraux, G. Leclert, and X. L. Zou, Plasma Phys. Contr. Fusion **38**, 1915 (1996).
[38] X. Garbet, Y. Sarazin, F. Imbeaux, P. Ghendrih, C. Bourdelle, Ö. D. Gürcan, and P. H. Diamond, Phys. Plasmas **14**, 122305 (2007).
[39] H. Y. Yuh, S. M. Kaye, F. M. Levinton, E. Mazzucato, D. R. Mikkelsen, D. R. Smith, R. E. Bell, J. C. Hosea, B. P. LeBlanc, J. L. Peterson, H. K. Park, and W. Lee, Phys. Rev. Lett. **106**, 055003 (2011).